ISSN 0021-3640, JETP Letters, 2011, Vol. 93, No. 4, pp. 226–232. © Pleiades Publishing, Inc., 2011.
Original Russian Text © N.A. Inogamov, V.V. Zhakhovskii, V.A. Khokhlov, V.V. Shepelev, 2011, published in Pis'ma v Zhurnal Eksperimental'noi i Teoreticheskoi Fiziki, 2011, Vol. 93, No. 4, pp. 245–251.

Superelasticity and the Propagation of Shock Waves in Crystals

N. A. Inogamov[a], V. V. Zhakhovskii[b, c], V. A. Khokhlov[a], and V. V. Shepelev[d]

[a] *Landau Institute for Theoretical Physics, Russian Academy of Sciences, Chernogolovka, Moscow region, 142432 Russia*
e-mail: nailinogamov@googlemail.com

[b] *Joint Institute for High Temperatures, Russian Academy of Sciences, ul. Izhorskaya 13/19, Moscow, 125412 Russia*

[c] *Department of Physics, University of South Florida, Tampa, Florida 33620, USA*

[d] *Institute for Computer Aided Design, Russian Academy of Sciences, Vtoraya Brestskaya ul. 19/18, Moscow, 123056 Russia*

Received January 21, 2011

The separation of a shock wave into an elastic precursor and a plastic wave is a characteristic phenomenon occurring only in solid media. The existence of the elastic shock wave at pressures $p \approx 10$ GPa, which is one or two orders of magnitude higher than the dynamic elastic limit, has been detected in recent numerical calculations and a femtosecond laser experiment. The plastic shock wave has no time to be formed in these ultrashort waves at $p \approx 10$ GPa. The processes of the formation and propagation of the elastic and plastic waves in aluminum at higher pressures obtained by means of femtosecond lasers have been analyzed in this work. It has been found that the elastic precursor survives even under the conditions when the pressure behind the plastic front reaches a giant value $p \sim 1$ Mbar at which the melting of the metal begins. It has been shown that superelasticity should be taken into account to correctly interpret the preceding laser experiments.

DOI: 10.1134/S0021364011040096

The invention of lasers capable of generating femtosecond pulses opens a way for investigating fast processes in matter. The development of the diagnostic methods for the subpicosecond timescale was of exceptional importance. With these methods, not only the generation, but also the measurement of fast processes initiated by a femtosecond laser became possible. The initiation and measurements are performed with a pair of ultrashort pulses using the stroboscope principle [1–7]. The first pulse in the pair is a high-power pump pulse and the second pulse is a weak probe pulse (pump–probe method). Both pulses are formed by means of the separation of a single initial pulse. They pass through paths with different optical lengths and arrive at a target at different times. The time delay t_{delay} of the arrival of the probe pulse with respect to the pump pulse is varied by the controlled variation of the optical length. Thus, a series of the phases and amplitudes of the probe pulse reflected from the place of the action of the pump pulse in t_{delay} is obtained. The phases and amplitudes provide information on time variation of the optical characteristics and on the fast evolution of heated matter. The pump pulses and the places of the irradiation of the target should be the same in different experiments of the series for success of the pump–probe method.

Femtosecond lasers are very efficient generators of shock waves in a condensed phase. They are used together with the pump–probe measurement method [1, 2, 4–7]. They easily expand the pressure range to values of 1–3 Mbar (1 Mbar = 100 GPa), which are reached even in the first experiments by Evans et al. [1]. In addition, femtosecond experiments allow for the investigations of early stages of the formation of compression shocks. These investigations cannot be performed by traditional tools (nanosecond lasers, pistons, etc.), which refer to other space–time scales. As a result, data on the strength of matter at record strain rates $\dot{V}/V \sim 10^9$ s^{-1} were obtained [6–9]. These data concern both the liquid phase (frontal ablation [8, 9]) and solid phase (rear spallation [6, 8]), the front side of the film is irradiated by the pump pulse. Investigations of the liquid phase by traditional methods are complicated.

Interesting results on the superelastic behavior of a crystal under ultrashort shock compression were obtained in [6, 7]. The continuation of the elastic Hugoniot adiabat far behind the commonly accepted Hugoniot elastic limit p_{HEL} was revealed. The p_{HEL} values are given in [10–13]; see also data on p_{HEL} in Fig. 4 in [6]. Agreement between the experiment [6] and theory [7] indicates that intense elastic shocks propagate in femtosecond experiments.

The results on superelasticity [6, 7] raise new problems, because they are strongly inconsistent with existing representations on the separation of the wave into elastic and plastic waves. It is clear that if the pres-

sure is increased, the plastic transition should appear even at scales ~1 μm considered in [6, 7]. Indeed, melting behind the wave front occurs in aluminum at a pressure of a piston of about 120 GPa, a piston velocity of about 5.5 km/s, and a shock velocity of about 13–14 km/s. In this case, the thickness of the melting front is about several interatomic distances and coincides with the thickness of the shock front (the problem of the transition to the liquid phase requires special discussion [14]). Large plastic deformations, which lead to the formation of the narrow plastic shock front, should obviously occur at somewhat lower pressures. New experiments and calculations are required to solve the problem of the elastic–plastic separation in aluminum at pressures of about 100 GPa.

In this work, we present the results of the simulation of the propagation of the compression wave with elastic–plastic separation. The numerical calculations allow for the correct interpretation of preceding experiments [1, 2, 5]. Analysis of these experiments indicates that the future experimental program should include experiments at intensities up to the optical breakdown of air at $I \sim 10^{14}$–10^{15} W/cm^2. A laser beam was focused on a target in the experiments reported in [1, 2, 4–6, 8] in air at normal pressure. It is necessary to use thin (200–700 nm), intermediate-thickness (1–2 μm), and thick (5–20 μm) metallic films. The two-temperature relaxation with hot electrons $T_e \gg T_i$ should be studied on thin films. The formation of the compression wave due to a sharp increase in the pressure in the heating region should be investigated on intermediate-thickness films. Finally, the propagation, modification, and attenuation of the elastic and plastic shock waves are analyzed on thick films. It is desired to compose pairs of measurements on free-standing films and measurements on films on glass. The laser pulse and film thickness in such a pair should be the same. The reason is that information on the processes inside the film is extracted from the trajectories of the motion of its rear boundary [1, 2, 5–8]. The motion of the boundary begins after the passage of the wave through the film to its rear side. The trajectories depend on the medium (air or glass) adjoining the boundary.

The glass plate supporting the metal film should be placed on the rear side of the film. Otherwise (heating of the film through glass), pressures are limited by a relatively low value of about 10 GPa in view of the optical breakdown of glass [2, 6]. The time t_{delay} is measured from the time of the arrival of the pump pulse at the front surface of the film. To determine the arrival time, a very thin (~10 nm) film is used [1, 2]. In addition, the energy F_{abs} absorbed in the target is determined by this method. This quantity is necessary for the accurate numerical simulation of the experiment (see Fig. 7 in [15]).

The essence of this work is illustrated in Fig. 1, where the $(V/V_0, p)$ plane is shown, where V_0 is the specific volume ahead of the wave front. The (1, 0) point on this plane corresponds to the state of the unperturbed crystal ahead of the wave. In the experiments with sufficiently large spatial scales,[1] the elastic Hugoniot adiabat is bounded by the curve segment between the (1, 0) and HEL points. The HEL point corresponds to the usual Hugoniot elastic limit [10–12]; $p_{HEL} \sim 0.04$–1 GPa for various kinds of aluminum (see Fig. 4 in [6]). The existence of the continuation of the elastic Hugoniot adiabat at $p > p_{HEL}$ was proved in [6, 7]. This continuation corresponds to the dotted curve between the HEL and HEL* points in Fig. 1. As was shown in [16], this continuation ends at the HEL* point with the pressure $p_{HEL^*} \approx 33$ GPa for the shock compression in the 111 direction. Aluminum single crystals with the concentration of vacancies per atom from zero to 0.001 were considered in [16]. Variation of this concentration does not affect the p_{HEL^*} value.

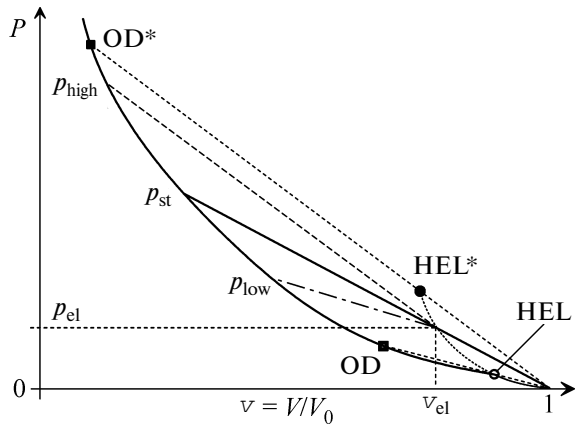

Fig. 1. Scheme of the mutual position of the elastic and plastic Hugoniot adiabats. The dotted segment HEL–HEL* is the metastable (with respect to the nucleation of dislocations) segment of the elastic Hugoniot adiabat. As follows from the slope of the Rayleigh straight lines, at $p_{high} > p_{st}$, the plastic shock moves more rapidly than the elastic precursor; at $p_{low} < p_{st}$, the plastic front moves more slowly than the elastic front.

In [16], the existence of a new regime of the propagation of the shock wave was revealed (this is regime III below). Including this regime, waves are classified into four regimes.

I. At sufficiently low pressures, a purely elastic stationary shock wave propagates. The Rayleigh straight line [10, 11, 17, 18] connecting the initial (1, 0) and final states ahead of and behind the wave front is a straight segment between the (1, 0) point in Fig. 1 and the point with a pressure in the range $0 < p < p_{HEL}$ on the elastic branch of the Hugoniot adiabat. The stationarity of the wave means that, first, the time evolution is obtained by the parallel translation of the wave

[1] Fractions of a millimeter and larger, see the comparison of the sizes in [6].

profile and, second, the propagation velocity and the slope of the Rayleigh straight line remain unchanged in time. The substance behind the wave front remains in the elastic state.

II. As pressure increases, a nonstationary two-wave regime appears; the elastic precursor and following slow plastic shock wave propagate [10–12]. The distance between the precursor and plastic front increases, because the velocity of the precursor is higher. On the $(V/V_0, p)$ plane in Fig. 1, regime II consists of two Rayleigh straight lines [10–12]. One line connects the (1, 0) and HEL points, and the second line connects the HEL and (v, p) points, where $v = V/V_0$. The (v, p) state in the pressure range $p_{HEL} < p < p_{OD}$ is on the segment of the plastic branch of the Hugoniot adiabat between the HEL and OD points (see Fig. 1). The point in this segment presents a plastically deformed state behind the plastic shock wave. The slope of the (1, 0)–HEL straight line is larger than the slope of the HEL–(v, p) straight line. These slopes become the same at the OD point at $p \longrightarrow p_{OD}$, because three points (1, 0), HEL, and OD in Fig. 1 lie on one line. The plastic adiabat near the OD point was analyzed in [19]. Slow plastic waves (piston velocity is $u_p \sim 100$ m/s) when the pressure p_p behind the plastic front is only slightly higher than p_{HEL} were considered in [20].

III. The stationary single-wave two-zone configuration corresponds to the straight line passing through the three points (1, 0), (v_{el}, p_{el}), and p_{st} in Fig. 1. The p_{st} point lies on the plastic Hugoniot adiabat. At a constant pressure on the piston p_{st} in the range $p_{OD} < p_{st} < p_{OD*}$, the width of the elastic zone, d_{el}, between the elastic and plastic fronts remains unchanged in time. In this regime, the velocities of the elastic and plastic fronts are the same and, correspondingly, there are two stationary compression regions, elastic and plastic. Since such a two-zone configuration moves as a single unit and remains unchanged in time, it should be considered as a stationary single-wave configuration. The state of the substance in the elastic zone in Fig. 1 is presented by the el point with the coordinates (v_{el}, p_{el}). This state is on the continuation of the elastic Hugoniot adiabat above the HEL point, which was found in [6, 7] and is shown by the thick dotted line in Fig. 1. The elastic substance is more rigid than the plastically transformed substance; correspondingly, the elastic adiabat is steeper than the plastic one. Therefore, the (1, 0)–el–p_{st} straight line first intersects the elastic Hugoniot adiabat. With a further increase in the pressure on the piston $p_{st} \longrightarrow p_{OD*}$, the thickness d_{el} of the elastic zone in the two-zone wave decreases. In this case, the pressure p_{el} in the elastic zone tends to the limiting value p_{HEL*}. The straight line passing through three points (1, 0), HEL*, and OD* corresponds to the wave in which the thickness of the elastic zone d_{el} is about the interatomic distance.

IV. At high constant pressure on the piston $p_p > p_{OD*}$, a purely plastic wave in which the elastic zone is almost absent propagates in the substance. In this regime, the wave forms a stationary single-wave configuration. Its Rayleigh straight line passes above the HEL* point in Fig. 1.

The earlier classification consisted of three regimes, I, II, and IV. The reasons why regime III remained unknown are as follows. The velocity of the shock wave D increases with the pressure of the piston p_p in pressure range I. As p_p increases in range II ($p_{HEL} < p_p < p_{OD}$), the velocity of the elastic precursor D_{HEL} is fixed and the velocity of the plastic front $D_{pl}(p_p)$ increases with p_p. Correspondingly, the distance between the fronts increases more slowly with p_p. In other words, the rate of the expansion of the elastic zone, $D_{HEL} - D_{pl}(p_p)$, decreases with the time and vanishes at $p_p \longrightarrow p_{OD}$. In this case, it was assumed that the velocity of the plastic shock wave at $p_p > p_{OD}$ (i.e., above the OD point in Fig. 1) is higher than the limiting propagation velocity D_{HEL} of the elastic signal and the plastic shock completely absorbs the elastic shock. For this reason, it was accepted that an increase in the pressure is accompanied by the transition at the OD point from regime II to regime IV with the single-wave configuration without any elastic zone. According to the calculations performed in [16], this is not the case; there is an intermediate regime III with a finite elastic zone.

Let us consider the problem of the generation of the two-zone wave (regime III) in the femtosecond experiment. It is necessary to take into account the physical specificity of the femtosecond laser generator of high pressures, namely, the formation of the substance layer with hot electrons overheated with respect to the crystal lattice ($T_e \gg T_i$). There are two main stages of the formation of the shock wave, the two temperature stage ($T_e \gg T_i$) and acoustic stage [7–9, 21]. The initial pressure profile is formed during two-temperature relaxation whose duration is $t_{eq} \approx 7$ ps, whereas the traveling shock wave is formed in the next interval $t_s \approx 10$ ps. These t_{eq} and t_s values refer to the experiment [1] on aluminum with the absorbed energy $F_{abs} = 2.6$ J/cm^2 and the pulse duration $\tau_L = 0.12$ ps. In this work, the intensity of the incident radiation $I_{inc} = 7.7 \times 10^{13}$ W/cm^2 corresponds to $F_{abs} = AF_{inc} = 2.6$ J/cm^2. The absorption coefficient $A(I_{inc}) = 1 - R = 0.28$ at this intensity is taken according to [22]. The relaxation time $t_{eq}(F_{abs})$ increases slowly with the energy F_{abs}. The introduced energy $F_{abs} = 2.6$ J/cm^2 is high; it is 40 times higher than the ablation threshold for aluminum [15]. The maximum electron temperature and pressure in time and space are 190 kK and 350 GPa. They are reached at the time of the end of the pump pulse. By the time $t = 2$ ps, the maximum pressure p_e decreases to 120 GPa. At the time $t = 3$ ps,

the maximum p_e and p_i values become equal to each other at a value of 90 GPa, although the internal electron energy at $t = 3$ ps is higher than the ion one. This circumstance is explained by the fact that the electron equation of state has the Gruneisen parameter $\Gamma = 2/3$ [17] that is smaller than the parameter $\Gamma \approx 2$ in the ion equation of state. With an increase in time $t > 3$ ps, the electron pressure gradually becomes dynamically insignificant.

Figure 2 shows the propagation of the compression wave in the film. The mass velocity profiles $u(x, t)$ were obtained by (line with small fluctuations) the molecular-dynamics (MD) simulation and (solid line) two-temperature hydrodynamic (2T-HD) simulation. The 110 crystallographic direction is oriented along the x axis coinciding with the propagation direction. The coordinate origin $x = 0$ is placed at the initial position of the frontal boundary of the film irradiated by the pump pulse. The film thicknesses in the calculations were 400 nm, 2 μm, and 9 μm. The concentration of randomly distributed vacancies in the initial crystal was 0.001 per atom, which is close to the real concentration at the aluminum melting point. Vacancies were introduced in order to approach the properties of the simulated crystal to a real crystal. The plastic equation of state is used in the 2T-HD code [7, 8, 23]; for this reason, the elastic zone in the elastic profile is absent. The elastic p_{el} and plastic p_{high} pressures (see Fig. 1) at the time shown in Fig. 2 are 20 and 93 GPa, respectively. Thus, the p_{el} value is about twice as high as the pressure reached in the experiments [6, 7].

The main result of this work follows from the comparison of the calculated and experimental [1] trajectories of the boundary of the 400-nm aluminum film with glass, see Fig. 3. The boundary is marked by segment B in Fig. 2. Figure 3 shows the displacement of the boundary, $\Delta x = x_{400}(t) - t_{400}(-\infty)$, where subscript 400 means that the position of the boundary before the arrival of hydrodynamic perturbation is $x_{400}(-\infty) =$ 400 nm. The small difference between acoustic impedances at the boundary was neglected in the calculations.

Let us compare the MD and 2T-HD simulations shown in Figs. 2 and 3. It can be seen how the elastic precursor affects the displacement law $\Delta x(t)$. The precursor region is marked by the two-sided arrow in Figs. 2 and 3. In contrast to the MD results, the elastic precursor is absent in the 2T-HD calculation, because the plastic solid model is used. The experimental data from [1] are shown by rectangles in Fig. 3 for the given pump pulse and target. It is remarkable that the same precursor is observed in the experiment! The calculated results for the outlet times of the precursor and plastic wave, as well as for the mass velocities behind the precursor and plastic shock (0.7 and 3–4 km/s, respectively, cf. the MD profile in Fig. 2) are in agreement with the respective experimental data. Thus, the experimental data confirm the existence of the elastic precursor ahead of the plastic shock with an amplitude of 1 Mbar. It is worth noting that the presence of the precursor was mentioned in [1, p. 3361], but its origin remained unclear.[2] At that time, it seemed improbable that the elastic precursor can exist ahead of waves with such a large amplitude.

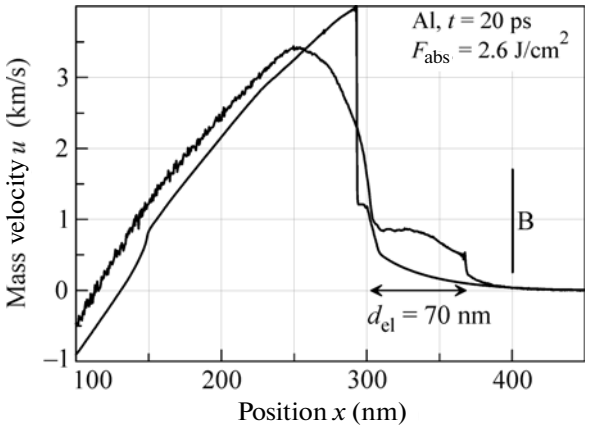

Fig. 2. (Line with small fluctuations) Molecular-dynamics simulation of the joint propagation of the elastic precursor and plastic front from the left to the right under the action of the pulse with intensity $I_{inc} = 7.7 \times 10^{13}$ W/cm^2 taken from [1]. The elastic zone with the thickness $d_{el} = 70$ nm between the front of the elastic shock wave (right shock) and plastic front (left shock) is marked by the horizontal two-sided arrow. The molecular dynamics results for the amplitude and width of the plastically compressed region are in agreement with the two-temperature hydrodynamic calculation. The interface between the Al film and glass is indicated by vertical segment B.

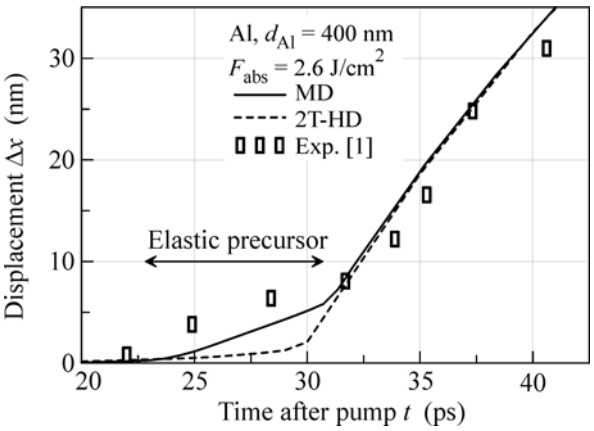

Fig. 3. Displacement of the interface with glass Δx in the process of the passage of the compression wave through the interface. The horizontal arrow marks the elastic precursor.

[2] As was shown in [1], the precursor cannot be attributed to radiative heating or fast electrons in this case.

To understand elastoplastic processes at large times, it is necessary to follow the evolution of the wave in thick aluminum films. To this end, using the 2T-HD and MD results for the action of a femtosecond laser pulse on 2- and 9-μm films, we analyze the recent experiments with 3–9-μm films [5].

The calculations indicate that the compression wave formed from the initial pressure profile is broken into two shock fronts. The elastic front is first formed in about 5 ps and the plastic front then appears in the next 10 ps. Thus, the separate breaking of two segments of the compression wave occurs with the formation of the elastic and plastic shock waves. These two shock waves are independent at the initial stage. The pressure on the front of the leading elastic shock wave at the time of its appearance is $p \approx 13$ GPa. The plastic shock wave is formed beginning with the melt boundary, where the pressure profile has a kink at a level of about 20 GPa. Thus, the pressure in the back part of the elastic zone, where it adjoins the plastic front is $p_{el} \approx 20$ GPa. The pressure at the peak of the plastic front is $p_{high} = 95$ GPa. In about 20 ps, the pressure becomes 20 GPa throughout the elastic zone and the velocity of the elastic shock wave becomes constant.

Further, such an elastoplastic configuration (fluctuating line in Fig. 2) continues to change for two reasons: first, the damping of the shock wave in the process of propagation through the target and, second, the interaction between the elastic and plastic waves. At the time shown in Fig. 2, the pressure in the plastic front is higher than the stationary value $p_{st} \approx 63$ GPa, which corresponds to the pressure $p_{el} \approx 20$ GPa in the stationary two-zone wave in regime III. For this reason, the Rayleigh straight line $p_{el} \longrightarrow p_{high}$ to the plastic state is steeper than the Rayleigh straight line $(1, 0) \longrightarrow p_{el}$ for the elastic shock (see Fig. 1). Correspondingly, the velocity of the plastic front is higher and it approaches the elastic shock. This leads to a gradual decrease in the thickness of the elastically compressed region.

It is interesting that at time intervals up to $t \approx 200$ ps, the pressure behind the plastic front decreases by a factor of 3, whereas the pressure $p_{el} \approx 20$ GPa behind the elastic shock and the velocity of this shock, 8.6–8.8 km/s, remain almost unchanged. In this case, the MD and 2T-HD calculations of the instantaneous position of the plastic shock wave and the pressure profile in the plastic region are in agreement with a high accuracy.

As was mentioned above, the pressure p_{high} behind the plastic shock in the time interval up to 70 ps is higher than the stationary value, $p_{high} > p_{st} = 63$ GPa (see the caption of Fig. 1). Correspondingly, the plastic front moves more rapidly than the elastic one and the thickness $d_{el}(t)$ decreases. The minimum value $d_{el} = 20$ nm is reached at $t = 70$ ps, when the pressures p_{high} and p_{st} become equal. At this time, the elastic and plastic segments of the Rayleigh straight lines form a single straight line (see Fig. 1). It is worth noting that the minimum thickness $d_{el} = 20$ nm is much larger than a lattice constant of 0.4 nm. Therefore, the unified Rayleigh straight line formed at $t \approx 70$ ps corresponds to the stationary two-zone wave in regime III, rather than in regime IV.

At times $t > 70$ ps, the pressure behind the plastic shock is lower than $p_{st}(p_{el} = 20\ \text{GPa}) = 63$ GPa. In this case, the angle between the segments of the elastic and plastic Rayleigh straight lines changes sign. In Fig. 1, these are the segments $(1, 0) \longrightarrow p_{el}$ and $p_{el} \longrightarrow p_{low}$. In this case, the elastic segment is steeper: the velocity of the elastic wave is higher, $p_{high} > p_{st}$ and $p_{low} < p_{st}$ (see Fig. 1). Therefore, the plastic transformation front propagates more slowly than the elastic precursor. In this case, the thickness $d_{el}(t)$ of the elastic zone begins to increase. For example, $d_{el} = 130$ nm at $t = 200$ ps. The corresponding plastic pressure $p_{low}(t = 200\ \text{ps})$ is 30 GPa.

The shape of the pressure and velocity profiles in the plastic wave is similar to triangular. The pressure behind the maximum of the profile decreases with almost spatially uniform instantaneous gradient $\partial p(x, t_{fix})/\partial x$. This triangle is broadened with time and its height decreases. The FWHM of the triangle $\Delta(t)$ and maximum pressure are 230 nm and 50 GPa at $t =$ 100 ps, 440 nm and 30 GPa at $t = 200$ ps, 700 nm and 20 GPa at $t = 500$ ps, and 1000 nm and 13 GPa at $t = 1000$ ps, respectively.

The width of the elastic zone $d_{el}(t)$ becomes equal to about the width $\Delta(t)$ when the shock wave penetrates to a depth of ~3 μm. At this time, the velocity of the plastic front decreases sharply to zero; i.e., the front stops. The thickness of the plastically transformed layer $\Delta_{pl}(F_{abs})$ is determined by the stop point and increases with F_{abs}. This property opens a way to the creation of plastically modified layers of the controlled thickness on the surface of a work piece. Note that the Δ_{pl} value estimated using commonly accepted low p_{HEL} values is much larger. The consideration of the stop of the plastic front indicates that the two-zone configuration of the elastic and plastic shock fronts after the stop is degenerated into an intense ($p_{el} \gg p_{HEL}$) purely elastic shock, which holds a high propagation velocity.

The experiments reported in [5] were carried out with an aluminum film at the same intensity 7.7×10^{13} W/cm^2 as in [1]. It was found that the average velocity of the wave propagating through the 9-μm film was about 9 km/s. Following the assumption made by the authors of [5] that the wave was a plastic shock wave, the pressure behind the plastic front at the end of the propagation through the 9-μm film should be about 70 GPa, according to the plastic Hugoniot adiabat. However, our calculations for this intensity of the laser pulse indicate that the pressure behind the

shock wave traveling a distance of 9 μm is as low as 13 GPa. Nevertheless, the shock wave travels the interval of 3–9 μm with a velocity of 8.3–8.7 km/s, because the substance in an elastic state composes the front of this wave. The high velocity of the elastic shock is determined by a steeper elastic Hugoniot adiabat. Thus, the concept of the completely plastic character of the shock wave led to an incorrect interpretation of interesting experiments performed in [5].

We emphasize that the existence of superelastic shock waves is a general phenomenon occurring in all crystalline substances. The existence of high velocities of the propagation of a shock wave in nickel films was detected in important work [2], where this phenomenon was not explained. The calculations of the elastic Hugoniot adiabats of nickel reported below provide the understanding of the unusually high velocity of the wave. To understand this property, it is necessary to assume that the shock wave has an elastic front. As a result, we will show that elastic, rather than plastic, shock waves were observed in the femtosecond experiments reported in [2].

The hydrodynamic and molecular dynamics calculations similar to those performed in [7] for aluminum require time-consuming computations. They have not yet been completed for nickel. For this reason, we use a numerical–analytical method for calculating elastic Hugoniot adiabats for nickel. Let us represent a shock adiabat for the velocity of the shock D in the form of the expansion $D/c = 1 + \sum_{i=1}^{\infty} a_i (u_p/c)^i$ in the piston velocity u_p, where c is the speed of sound ahead of the shock wave. Applying the Mathematica package for symbolic manipulation to the conditions of the conservation of the mass, momentum, and energy fluxes on the shock front [17, 18], we obtain (expressions for higher-order coefficients a_i are lengthy and not presented here)

$$a_1 = \frac{1 + A_1}{2}, \quad a_2 = \frac{1 + 2A_1 - 3A_1^2 + 4A_2}{8} + \Gamma_0 \frac{a_1}{6}. \quad (1)$$

Here, we used the expansions

$$p_c(\rho) = K \sum_{n=0} A_n x^{n+1},$$

$$\Gamma(\rho) = \sum_{m=0} \Gamma_m x^m$$

of the cold pressure curve and Gruneisen parameter, respectively, where $K = \rho c^2$, ρ is the density ahead of the shock wave, and $A_0 = 1$. The compression degree in the shock wave is $\rho_{SW}/\rho = 1 + x$. The formula for a_1 coinciding with the first of Eqs. (1) was given in [24].

The cold curves for nickel and aluminum for uniform and uniaxial compressions in the 100, 110, and 111 directions were obtained from the quantum-mechanical density functional calculations using the VASP and ABINIT packages (the presentation of these quantum calculations is beyond the scope of this paper). The coefficients $\Gamma_0 = 1/3 + A_1$, $\Gamma_1 = A_1 - 2A_1^2 + 3A_2$, etc., were calculated by the Slater formula [25] from the cold curve. The plastic Hugoniot adiabats thus obtained for aluminum ($c = 5.4$ km/s, $a_1 = 1.4$) and nickel ($c = 4.6$ km/s, $a_1 = 1.4$) are in agreement with the experimental data [24] with accuracies of 1 and 3% in c and a_1. Analysis shows that the corrections a_2 and a_3 are insignificant in the range of interest (in view of elastic shock waves) up to $u_p \sim 2$ km/s. For the elastic Hugoniot adiabat of aluminum for the 111 direction, we obtained $a_1 = 1.7$ in agreement with the value $a_1 \approx 1.75$ from the molecular dynamics data [7]. The calculations for nickel give $(c, a_1) = (5.3$ km/s, $0.7)_{100}$, (6 km/s, $1.7)_{110}$, and (6.2 km/s, $1.4)_{111}$.

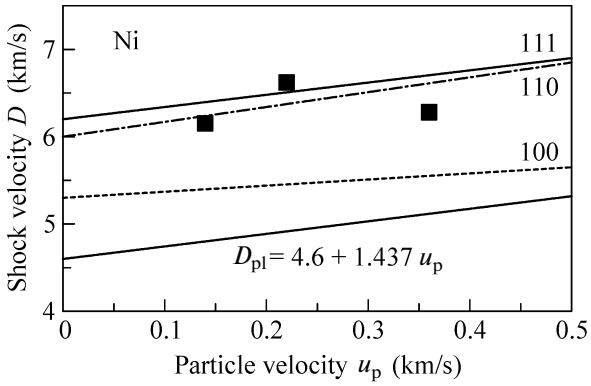

Fig. 4. Experimental points taken from [2] in comparison with the (100, 110, and 111) elastic and plastic Hugoniot adiabats.

Figure 4 shows the elastic Hugoniot adiabats of nickel $D_{ijk} = c_{ijk} + a_{ijk}u_p$, where $ijk = 100$, 110, and 111, along with the plastic adiabat $D_{pl} = 4.6 + 1.437u_p$ (velocities are in kilometers per second) and the experimental points taken from Table 1 in [2]. As is seen, the points of the femtosecond experiment are far from the plastic Hugoniot adiabat. These points are above the elastic Hugoniot adiabat for the 100 direction and below the elastic Hugoniot adiabats for the 110 and 111 directions. Therefore, elastic shock waves were observed in the experiments reported in [2]. These waves exist at pressures much higher than the p_{HEL} for nickel.

CONCLUSIONS

The results of the detailed numerical simulation of the formation and propagation of ultrashort shock waves generated in metals by a femtosecond laser have been reported. It has been shown that such shock waves can have two shock fronts and a wide elastic

zone of the uniaxially compressed crystal between the elastic and plastic shock fronts.

The work of N.A.I. and V.A.Kh. was supported by the Russian Foundation for Basic Research, project no. 09-08-00969-a. The molecular-dynamics simulation was performed at Ranger and Kraken NSF TeraGrid supercomputers and was supported by grant no. TG-MCA08X040.

REFERENCES

1. R. Evans, A. D. Badger, F. Fallies, et al., Phys. Rev. Lett. **77**, 3359 (1996).
2. K. T. Gahagan, D. S. Moore, D. J. Funk, et al., Phys. Rev. Lett. **85**, 3205 (2000).
3. V. V. Temnov, K. Sokolowski-Tinten, P. Zhou, and D. von der Linde, J. Opt. Soc. Am. B **23**, 1954 (2006).
4. M. B. Agranat, N. E. Andreev, S. I. Ashitkov, et al., Pis'ma Zh. Eksp. Teor. Fiz. **85**, 328 (2007) [JETP Lett. **85**, 271 (2007)].
5. Li Huang, Yanqiang Yang, Yinghui Wang, et al., J. Phys. D **42**, 045502 (2009).
6. S. I. Ashitkov, M. B. Agranat, G. I. Kanel', et al., Pis'ma Zh. Eksp. Teor. Fiz. **92**, 568 (2010) [JETP Lett. **92**, 516 (2010)].
7. V. V. Zhakhovskii and N. A. Inogamov, Pis'ma Zh. Eksp. Teor. Fiz. **92**, 574 (2010) [JETP Lett. **92**, 521 (2010)].
8. M. B. Agranat, S. I. Anisimov, S. I. Ashitkov, et al., Pis'ma Zh. Eksp. Teor. Fiz. **91**, 517 (2010) [JETP Lett. **91**, 471 (2010)].
9. B. J. Demaske, V. V. Zhakhovsky, N. A. Inogamov, and I. I. Oleynik, Phys. Rev. B **82**, 064113 (2010).
10. G. I. Kanel', S. Razorenov, and V. E. Fortov, *Shock-Wave Phenomena and the Properties of Condensed Matter* (Springer, 2004).
11. *High-Pressure Shock Compression of Solids*, Ed. by J. R. Asay and M. Shahinpoor (Springer, 1993).
12. G. I. Kanel', V. E. Fortov, and S. V. Razorenov, Usp. Fiz. Nauk **177**, 809 (2007) [Phys. Usp. **50**, 771 (2007)].
13. T. Antoun, L. Seaman, D. R. Curran, et al., *Spall Fracture* (Springer, 2003).
14. M. M. Budzevich, V. V. Zhakhovsky, I. I. Oleynik, and C. T. White, Phys. Rev. B (in preparation).
15. S. I. Anisimov, N. A. Inogamov, Yu. V. Petrov, et al., Appl. Phys. A **92**, 797 (2008).
16. V. V. Zhakhovsky, M. M. Budzevich, N. A. Inogamov, et al., Science (in preparation).
17. L. D. Landau and E. M. Lifshitz, *Course of Theoretical Physics*, Vol. 6: *Fluid Mechanics* (Nauka, Moscow, 1986; Pergamon, New York, 1987).
18. Ya. B. Zel'dovich and Yu. P. Raizer, *Physics of Shock Waves and High-Temperature Hydrodynamic Phenomena*, Vols. 1 and 2 (2nd ed., Nauka, Moscow, 1966; Academic, New York, 1966, 1967).
19. A. M. Molodets, Teplofiz. Vysok. Temp. **40**, 521 (2002).
20. J. N. Johnson and L. M. Barker, J. Appl. Phys. **40**, 4321 (1969).
21. N. A. Inogamov, V. V. Zhakhovsky, S. I. Ashitkov, et al., Contr. Plasma Phys., DOI: 10.1002/ctpp.201010111.
22. D. F. Price, R. M. More, R. S. Walling, et al., Phys. Rev. Lett. **75**, 252 (1995).
23. A. V. Bushman, G. I. Kanel', A. L. Ni, and V. E. Fortov, *Intense Dynamic Loading of Condensed Matter* (Taylor Francis, London, 1993).
24. R. F. Trunin, in *High-Pressure Shock Compression of Solids VII*, Ed. by V. E. Fortov et al. (Springer, New York, 2004).
25. J. C. Slater, *Introduction to Chemical Physics* (McGraw-Hill, New York, London, 1939).

Translated by R. Tyapaev